Ultrastructural Visualization of 3D Chromatin Folding Using Serial Block-Face Scanning Electron Microscopy and In Situ Hybridization (3D-EMISH)

Paweł Trzaskoma[1,8], Błażej Ruszczycki[1,8], Byoungkoo Lee[2,8], Katarzyna K. Pels[1], Katarzyna Krawczyk[1], Grzegorz Bokota[3], Andrzej A. Szczepankiewicz[1], Jesse Aaron[4], Agnieszka Walczak[1,5], Małgorzata A. Śliwińska[1], Adriana Magalska[1], Michal Kadlof[3], Artur Wolny[1], Zofia Parteka[3], Sebastian Arabasz[6], Magdalena Kiss-Arabasz[6], Dariusz Plewczynski[3,7], Yijun Ruan[2*], Grzegorz M. Wilczyński[1*]

[1] Nencki Institute of Experimental Biology, Polish Academy of Sciences, Warsaw, Poland

[2] The Jackson Laboratory for Genomic Medicine, Farmington, CT, USA

[3] Center of New Technologies, University of Warsaw, Warsaw, Poland

[4] Janelia Research Campus, Howard Hughes Medical Institute, Ashburn, VA, USA

[5] Department of Gene Expression, Institute of Molecular Biology and Biotechnology, Faculty of Biology, Adam Mickiewicz University, Poznan, Poland

[6] Łukasiewicz Research NETWORK – PORT Polish Center for Technology Development, Wrocław, Poland

[7] Mathematics and Information Science, Warsaw Technical University, Warsaw, Poland

[7] equal contribution as co-first authors

* corresponding authors: Grzegorz M. Wilczyński (g.wilczynski@nencki.gov.pl), Yijun Ruan (Yijun.Ruan@jax.org)

Abstract

The human genome is extensively folded into 3-dimensional organization, yet the detailed 3D chromatin folding structures have not been fully visualized due to the lack of robust and ultra-resolution imaging capability. Here, we report the development of a novel electron microscopy method that combines serial block-face scanning electron microscopy with in situ hybridization (3D-EMISH) to visualize 3D chromatin folding at targeted genomic regions with ultra- resolution (5x5x30 nm in xyz dimensions, respectively). We applied 3D-EMISH to human lymphoblastoid cells at a 1.7 Mb segment of the genome and visualized a large number of distinctive 3D chromatin folding structures in ~~high~~ ultra-resolution. We further quantitatively characterized the reconstituted chromatin folding structures by identifying sub-domains, and uncovered a high level of heterogeneity in chromatin folding ultrastructures, suggestive of extensive dynamic fluidity in 3D chromatin states.

Introduction

How the two-meter-long human genome is folded into the micrometer-sized nuclear space is an important question in biology. Indeed, specific three-dimensional (3D) organization of chromosomal folding has been shown to have a profound impact on genome functions such as gene transcription[1] and DNA replication[2]. To investigate the detailed structures of 3D genome organization, two general approaches have been developed and applied - sequencing-based mapping and microscopy-based imaging. Mainstream 3D genome mapping methods such as Hi-C[3,4] and ChIA-PET[5] detect pairwise long-range chromatin interactions by chromatin proximity ligation followed by high throughput sequencing and mapping to the reference genome, thus inferring long-range chromatin contacts and rendering the 3D configuration of the genome. However, 3D genome mapping data are derived from millions of cells[6] and provided an average view of genome folding. Specifically

the techniques revealed smaller subunits of chromosome territories – topologically associated domains (TADs by Hi-C)[7–9] and chromatin contact domains (CCDs by ChIA-PET)[10], demarcated by multiple binding sites for CTCF protein[11]. However, even though the contact probabilities are clearly displayed, the mapping data lack physical scale (e.g. in micrometers). To overcome these limitations, microscopy can be used to visualize the actual genome architecture and metric scale in various spatiotemporal resolutions in individual nuclei with different DNA staining methods. Standard fluorescence microscopy has an optical resolution of about 250 nm[12] and has been applied to image mammalian nuclei, successfully establishing the concept of chromosome territory[13] showing chromosomal morphologies in different cell cycle phases, and is also routinely used in cytogenetics to study abnormal chromosomes[14]. Recently, a super-resolution fluorescence light microscopy (20x20 nm in xy dimensions, 50 nm in z) with sequence-specific DNA binding probes was applied to visualize specific chromatin folding structures for a 10 – 500 Kb target genomic region in Drosophila cells[15,16] and 1.2 – 2.5 Mb target genomic region in human cells[17]. However, this method has a limit in z-dimension image depth (up to 3μm)[17], and thus larger 3D chromatin structures beyond this limit would be truncated or lost**.** Electron microscopic in situ hybridization (EMISH) using biotin-labeled DNA probes coupled with diaminobenzidine staining has been used to image chromosomal DNA in the nuclei[18]. When standard FISH protocols are used in electron microscopy (EM) study, severe artefacts have been attributed to formamide and high temperature treatment[19]. However, volume (3D) EM approaches – Serial Block-Face Scanning Electron Microscopy (SBF-SEM){Citation} and Focused Ion Beam Scanning Electron Microscopy (FIB-SEM) Hoang et al. 2017 were used with success in studies of global architecture of cell nuclei. SBF-SEM can reach a resolution ~ 5x5 nm in xy, while resolution in z depends on a thickness of cut ultrathin slices, and FIB-SEM achieves a resolution down to ~ 3 nm in all dimensions. The most recent effort in using EM for imaging chromatin structure is EM tomography with even higher resolution (1x1x1 nm), in which

photo-oxidized label is used to mark all DNA and to visualize the overall chromatin structures for 3D imaging in the nucleus[20], but within a limited depth at z-axis (250nm). Nonetheless, our ability to visualize 3D chromatin folding structures in high quality ultra-resolution remains inadequate, hampered in particular by the lack of sequence specificity and low depth of imaging in the z-dimension.

To achieve ultra-resolution visualization of sequence-specific 3D chromatin folding structures, we developed 3D-EMISH, which combines advanced in situ hybridization using biotinylated DNA probes[21] with silver staining and serial block-face scanning electron microscopy (SBF-SEM)[22,23]. The serial z-stack EM images can be assembled computationally into a 3D conformation of the targeted genomic region with a resolution of 5x5 nm in the xy-plane and 30 nm in the z-axis. We applied 3D-EMISH to visualize a specific chromatin folding location in the human genome, and analyzed more than 200 distinctive 3D chromatin structures derived from individual nuclei of human lymphoblastoid cells. To our knowledge, this is the first time when SBF-SEM is applied for imaging specific chromatin folding structures.

Results

The 3D-EMISH methodology

Our method includes 3D preservation of the nuclei, in situ hybridization of specific DNA probes, serial scanning by EM, and imaging data analysis to reconstruct the spatial models of chromatin folding structures (Fig. 1a).

In the first step of the 3D-EMISH protocol, cells were fixed with 4% freshly-made paraformaldehyde, and then embedded in a thrombin-fibrinogen clot, postfixed,

cryoprotected in 30% sucrose, and frozen in dry ice-cooled isopentane. The embedded clots (less than 5mm in size) were cut into 40 µm-thick sections in the freezing microtome.

The next step in 3D-EMISH is in situ hybridization (ISH). The free-floating 40 µm-thick sections were incubated with the biotinylated DNA probes targeting a specific genomic region of interest. The signals of the biotinylated DNA probes for EM detection were processed with the use of 1.4nm-thick streptavidin-conjugated fluoronanogold particles and subsequent silver enhancement. The procedure of silver enhancement was experimentally optimized to obtain electron dense 4-5 nm diameter granules as the smallest items (Supplementary Fig. 1a-c). To optimize chromatin ultrastructure preservation, we performed a set of control in situ hybridization (ISH) reactions. Using transmission electron microscopy (TEM), we assessed in details the influence of potentially harmful factors associated with the ISH procedure. We found, that the permeabilization with Triton X-100 causes negligible changes in chromatin structure (Compare the Supplementary Fig. 1d and 1e) . Formamide and high temperature did evoke some damage in the form of small, empty spaces in the nucleoplasm and a significant diminution of the condensed chromatin layer beneath the nuclear envelope (Supplementary Fig. 1f). However, surprisingly, we found that the factor most significantly disturbing the chromatin ultrastructure was the incubation of the sample with dextran sulfate (Supplementary Fig. 1f), causing changes similar to that described by Solovei et al.[19] after all hybridization steps. Dextran sulfate is typically added in ISH to increase the probe concentration and the hybridization reaction speed. The addition of dextran sulfate caused the formation of extensive filamentous network in the nucleoplasm, and the total lack of the condensed chromatin beneath the nuclear envelope, at the ultrastructural level.

To ascertain, that the changes observed by us, in fact occurred in the chromatin, we performed a specific DNA staining with terminal deoxynucleotidyl transferase (TdT) according to M. Thiry (cit). (Supplementary Figure S2). This method utilizes TdT to add

labelled nucleotides to the free DNA ends, formed by ultrathin cutting, that are subsequently detected by immunogold staining. This experiment demonstrated that the extensive filamentous network formed after addition of dextran sulfate was overlaid by colloidal gold particles indicating the DNA location. Some particles were also found in the cytoplasm, what might suggest the loss of nuclear membrane integrity. We observed that the lack of dextran sulphate in ISH had only a minor impact on hybridization efficiency (Supplementary Fig. 1h-i). However, it led to somewhat increased background (especially at the surface of the sliced section). The 40 µm-thick sections were stained with uranyl acetate and tannic acid, followed by dehydrating and flat-embedding in an epoxy resin. Because uranyl acetate stains nucleic acids and proteins broadly, its inclusion in 3D-EMISH enabled us to visualize the overall nuclear space in relation to the target chromatin structure (Fig. 1a).

One block of the embedded specimens (usually less than 1mm in width) was placed in the chamber of a SBF-SEM (Supplementary methods, Zeiss Sigma VP) equipped with a built-in ultramicrotome (Gatan 3View). The specimen block was consecutively sliced one layer at a time at 30-50nm intervals, and the exposed surfaces of the specimen were serially scanned in a field of 8192x8192 pixels (approximately 1700 μm^2, when a pixel size is 5 nm) to obtain volumetric data including the specific 3D-EMISH signals. The specimen was sliced again for the next round of signal acquisition and so forth. This cycling process of slicing-scanning was performed hundreds of times to generate z-stack images in a 3D-EMISH experiment (Fig. 1a).

Since all in situ hybridization reactions result in non-specific background[21], the 3D-EMISH signals in each slice also included punctate patterns of staining that we deemed likely to be noise. We reasoned that the real signals from the targeted chromatin would be in continuation in multiple layers of the Z-stack images, whereas the background signals would not be connected in the Z-stacks (Fig. 1b). Therefore, we developed an image processing algorithm based on multi-layer connectivity to retain true chromatin positive signals and

remove false-positive ones. After filtering out the background noise, the chromatin signals were assembled to reconstruct the 3D chromatin folding structure in 3D EM resolution for the targeted genomic region (Fig. 1c-d).

3D EM resolution of chromatin folding structures captured by 3D-EMISH

We applied 3D-EMISH to investigate chromatin folding structures in the genome of the human lymphoblastoid cell line GM12878. This cell line has been extensively studied for epigenome and 3D genome mapping[7,10]. At a specific genomic region (chr7: 141,547,153 – 143,237,066, 1.7Mb length, hg38), three distinctive loop domains were inferred by extensive CTCF ChIA-PET data (Fig. 2a). RNAPII ChIA-PET and RNA-Seq further suggested that the genes in the first loop domain and part of the third domain are in active transcriptional loops. To confirm the presence of the chromatin loop domains inferred by these sequencing-based approaches, we designed and produced biotinylated DNA probes derived from 11 BAC clones to cover this region for 3D-EMISH experiments (Fig. 2a). To test the hybridization efficiency of the probes to the target genomic region, we also generated two-color fluorescence probes from the BAC clones that could help distinguish the three domains (Fig. 2a). Subsequently, we performed 3D FISH imaging analysis using confocal microscopy, and validated that these probes were efficient and highly specific (Fig. 2b).

Using the biotinylated DNA probes, we performed 3D-EMISH experiments in GM12878 cells at exponential growth phase. We performed two independent experiments using two different EM settings, producing image voxel size of 7x7x50 nm in replicate 1 and 5x5x30 nm in replicate 2. The sample cubical blocks were analyzed by a series of 300 (replicate 1) or 600 (replicate 2) slicing and scanning cycles, rendering consecutive 50 nm (replicate 1) or 30 nm (replicate 2) sections, respectively. One specimen, typically about 1000x1000x40 µm, included tens of thousands of cells. However, the cubic volumes that

were scanned by EM microscopy were much smaller and they were 3200 μm^2 in xy and 15 µm in z for replicate 1, and 1700 μm^2 in xy and 18 µm in z for replicate 2. Each of the Z-stack images could capture a cross section of about 10 - 30 cell nuclei, intact or truncated (Fig. 2c). After signal de-noising and assembling, the outline of a nuclear framework and the specific chromatin objects could be visualized respectively based on the uranyl acetate and the silver staining signals (Fig. 2d). From two independent 3D-EMISH experiments, a total of 166 nucleus image-stacks were obtained. Most of them (140) were truncated nuclei and contained from 1 to 4 specific target signals, whereas 26 nuclei were intact with 2 or 4 specific chromatin targets (Fig. 2e), suggesting that the cells were possibly in G1 phase (2 copies of target region) or S-G2 phase of the cell cycle.

To compare 3D-EMISH with super-resolution microscopy, we applied iPALM[24] and visualized the same targeted chromatin structures using iPALM-specific probes tagged with two-color “blinking” fluorophores for the same genomic region in GM12878 cells (Supplementary Fig. 2). The iPALM 3D image structure showed about 4-fold lower resolution (20x20 nm in xy) than the 3D-EMISH images. In addition, the depth of an iPALM image at z-dimension was limited at 750nm[25], thus capturing only incomplete chromatin structures, even though isolated nuclei were used for iPALM imaging to reduce the depth of cell specimen. Thus, 3D-EMISH not only provided higher resolution of chromatin images at xy plane than iPALM, but also provided greater depth at the z-axis than iPALM, enabling visualization of complete 3D chromatin folding structures. However, the use of two different fluorophores in iPALM allowed determination of the orientation of the chromatin folding structure along the linear DNA strand.

Heterogeneity of chromatin folding structures in 3D EM resolution

In total, we captured 229 distinct chromatin folding structures (Supplementary Fig. 3) for the 1.7 Mb region from 166 nuclei examined in our 3D-EMISH experiments. At first glance, it appeared that the chromatin folding structures at this region in GM12878 cells varied from having a single domain to multiple sub-domains. To further quantitatively analyze the structural features, we developed a computational algorithm to characterize potential chromatin folding properties. First, we aligned each of the reconstructed 3D chromatin structures along with its principal axes, by orthogonalization of the structure inertia tensor. This representation allows clear dissection of the chromatin signals in more detailed folding structures (Fig. 3a). Next, we calculated the local density centers in each chromatin structure, followed by diffusing the density from the centers to demarcate the boundaries and to identify distinctive domains in the 3D-EMISH structures (Fig. 3a). For example, in the three different 3D-EMISH structures (sID50, sID12, sID42), one, two and three local density centers were identified, respectively, corresponding to morphological domains (Fig. 3b and Supplementary Fig. 4). The sub-domains in each 3D-EMISH structure were demarcated by different colors (Fig. 3c).

Applying this algorithm to the aforementioned 229 chromatin folding structures captured by 3D-EMISH, we analyzed the detailed chromatin domain composition in each of the structures (Fig. 4a and Supplementary Fig. 5). Interestingly, we identified 58 (25%) 3D-EMISH structures with one domain, 90 (39%) with two, 70 (31%) with three, and 11 (5%) with four or five domains (Fig. 4b). Only two structures were identified as five domains, and we merged them with four domains structure group for our statistical analysis. Remarkably, the structures with multiple sub-domains accounted for a combined 75% of all the structures, which is approximately in line with the ChIA-PET mapping data (Fig. 2a). To further characterize these chromatin folding structures, we measured the volume and the surface area for each. These measurements showed that the chromatin structures with one domain had the smallest volume and surface values, and the structures with more than one domain

showed increased values along with the numbers of domains (Fig. 4c-d). We also calculated the form factor (volume/surface; see the detailed formula in Online Methods) for each structure, which showed the same trend as the other measurements, i.e. single-domain structures had the lowest form factor value (Fig. 4e).

Taken together, our imaging analyses suggest that the small percentage of one-domain structures captured in our data most likely exemplify condensed chromatin folding states, whereas the majority of the structures contained sub-domains and could represent loose chromatin folding characteristics with various substructures for different domain functions during interphase in B lymphoblastoid cells. It is noteworthy that many of the structures captured in this 3D-EMISH study showed three domains, consistent with our ChIA-PET data based on bulk cells (Fig. 2a). Furthermore, the ultra-resolution details unraveled a high level of heterogeneity of chromatin folding structures within this 1.7 Mb region. Strikingly, each individual chromatin ultrastructure, even those having the same number of sub-domains, showed a uniquely distinctive chromatin folding conformation (Fig. 4a; Supplementary Fig. 5).

Discussion

We have demonstrated 3D-EMISH as an effective imaging technique with ultra-resolution (5x5x30nm) capability to capture specific 3D chromatin folding structures in individual nuclei, superior to the current super-resolution 3D visualization by fluorescence light microscopy. The use of in situ hybridized DNA probes targeting the specific genomic regions provided specificity of folding structures. The use of SBF-SEM enabled single-digit nanometer resolution for the xy dimension. More advantageously, it allowed collecting z-stack images up to 18 micrometers in total depth, which is not possible by super-resolution microscopy, such as iPALM and STORM, because of their optical image depth limit. Additionally, each 3D-

EMISH experiment could analyze large numbers of chromatin structures from multiple cells simultaneously, and multiple experiments could be robustly performed for analyzing large numbers of individual cells. The inclusion of *en-bloc* staining with uranyl acetate used in 3D-EMISH resulted in relatively weak counterstaining of the nuclear area, thus providing additional benefit for outlining the spatial location of the target structure in relation to the nuclear border.

Recently, another EM approach, ChromEMT, has been introduced for chromatin structure analysis[20]. It uses photo-oxidized diaminobenzidine polymers and OsO_4 fixation, rendering a detection system size of about 1 – 2 nm. The method is also characterized by the highest available resolution (less than 1 nm in xy) and, due to utilizing EM tomography, about 1 nm in z. Therefore, ChromEMT can visualize single DNA polymer loops. However, the ChromEMT approach stains all DNA in nuclei, and thus lacks sequence-specificity and allows investigation of only 250 nm-thick section. In contrast, 3D-EMISH uses DNA probes to target a given genomic region of interest with high specificity, and the obtained 3D images can be immediately correlated with the available genomic mapping data, thus providing novel insights into potential structure-function relationships. Nonetheless, these two EM approaches are complementary to each other for ultra-resolution visualization of the global nature of chromatin organization and specific features of chromatin folding.

The ultrastructures of 3D chromatin folding domains unraveled by 3D-EMISH are ultra-resolution snapshots of the target genomic region from individual cells. All of these 229 snapshots showed a dynamic nature of chromatin folding. The ultra-resolution nature of the 3D-EMISH structures displayed a high level of heterogeneity in chromatin folding with respect to different volume and shape even of the two copies of chromatin fold in the same nucleus. The variations in the 3D chromatin folding structures within the 229 images may be a reflection of spatiotemporal dynamics and potential functional properties such as transcription activity and epigenetic state[15], and also cell cycle phase[20,26]. Heterogeneity in

the chromatin organization is observed at different levels. For example, we have shown different conformations of chromosome 1 even within the same nucleus[10]. There are also results obtained in human cells showing high variability in the physical distances between selected genomic loci (cit) and variability in the organization of chromatin domains[16]. Moreover, studies of transcription reveal expression heterogeneity (cit). Also in the same cells that we studied – GM12878, heterogeneity was shown using single cell sequencing approaches – scATAC-Seq and scRNA-Seq when compared to bulk studies. It suggests that variability observed by us and others could interplay with transcriptional activity. Nevertheless, the relation between dynamic changes of chromatin structure and stochasticity in gene expression is not yet fully understood (cit).

ONLINE METHODS

Cell culture

GM12878 (human lymphoblastoid) cells were cultured in RPMI-1640 medium (Sigma) with addition of 2 mM GlutaMax (Gibco), 15% FBS (Gibco), 100 U/ml penicillin and 100 µg/ml streptomycin (Gibco), at 37°C; 5% CO_2.

DNA probes used in in situ hybridizations

The DNA probe was designed based on BAC (bacterial artificial chromosome) clones obtained from CHORI (Children's Hospital Oakland Research Institute) and verified with PCR. The designed 11 BACs (CH17-148N23, CH17-120P14, CH17-417P16, CH17-265E23, CH17-52M16, CH17-310K12, CH17-121M24, CH17-326A22, CH17-215B18, CH17-450A09, CH17-227I19) covered our genomic target region in human chromosome 7: 141,547,153 - 143,237,066, in hg38. After isolating DNA from BACs using alkaline lysis method, DNA

amplification was performed using the Illustra GenomiPhi V2 DNA Amplification Kit (GE Healthcare Life Sciences) and DNA labelling with biotin using the Biotin-Nick Translation Mix (Roche) and digoxigenin with the DIG-Nick Translation Mix (Roche). The product of reaction was mixed with human competitor DNA (Applied Genetics Laboratories, Inc.), salmon sperm DNA (Invitrogen), absolute ethanol and incubated 2 hours at -20□C. Then, the probe was centrifuged, dried with a vacuum centrifuge and dissolved in 100% formamide (overnight; 37□C; with shaking). To obtain a ready-to-use probe, a 4xSSC buffer was added to the probe dissolved in 100% formamide (1:1; finally probe dissolved in 50% formamide in 2xSSC). In the case of light microscopy, dextran sulphate was also added to final concentration 10%.

Cell preparation for confocal microscopy

The cell pellet was fixed with 4% paraformaldehyde in PBS (10 min; RT), washed with PBS and cells were spun down onto a glass slide ($1x10^5$ cells/13mm coverslip) using a cytocentrifuge.

Cell preparation for iPALM

Nuclei were isolated (Sigma; Nuclei Isolation Kit: Nuclei EZ Prep), fixed with 4% paraformaldehyde in PBS (10 min; RT) and attached onto coverslips (with fiducial markers) washed earlier with 1M KOH (20 min), rinsed with water and coated with 0.01% poly-L-Lysine for 20 min (Sigma).

DNA-FISH protocol

3D DNA-FISH was performed according to Cremer et al.[27], with modifications. After blocking of endogenous biotin (Vector Laboratories; SP-2001), the cells were permeabilized with 0.5% Triton X-100 (Sigma) in PBS (RT, 20 min). To augment permeabilization, the cells were immersed in a cryoprotectant solution (20% glycerol in PBS, RT, 2h) followed by their repeated freezing-thawing above the surface of the liquid nitrogen (4 x 30 sec). Subsequently, the cells were washed in PBS containing 0.05% Triton X-100 (Sigma) (RT, 3 times for 5 min), treated with 0.1 N HCl (RT, 5 min), washed again in 2xSSC at 37□C and incubated in 50% formamide in 2xSSC (4□C, overnight). On the next day, the probe was added, the samples were denatured (5 min, 80□C) and hybridized (48h, 37□C). Then, the samples were washed with 2xSSC (3 x 5 min; 37□C; with shaking), 0.1xSSC (3 x 5 min; 60□C; with shaking),

rinsed briefly with 0.2% Tween (Sigma) in 4xSSC and incubated with blocking solution- 4% BSA (Sigma), 0.2% Tween (Sigma), 4xSSC (1h, 37□C) following incubation with the detection system for confocal microscopy or iPALM.

Two-color DNA-FISH experiment - confocal microscopy

DNA probe signals were captured by two-steps system detection of biotin- labelled probe with avidin-AlexaFluor488 (Molecular Probes) and anti-avidin-FITC (Sigma), and two-steps system detection of digoxigenin- labelled probe with anti-digoxigenin-rhodamine produced in sheep (Roche) and secondary antibody donkey anti sheep-TRITC (Jackson ImmunoResearch). DNA was counterstained using Hoechst 33342 (Molecular Probes), and samples were mounted with Vectashield (Vector Laboratories).

Confocal microscopy imaging and post-processing

The samples were imaged with Zeiss LSM 780 microscope, using a 63x oil immersion objective (NA 1.4) and a 405 nm diode laser, 488 nm line of argon laser, 561 nm DPSS diode laser, 633 nm HeNe laser; with 70 nm xy pixel size, and 210 nm z-spacing. The image-stacks were deconvolved using Huygens software (SVI) with the maximum-likelihood estimation (MLE) algorithm. FISH signals imaged by confocal microscopy were segmented based on the threshold and reconstructed using Imaris (Bitplane) software.

Two-color DNA-FISH experiment - iPALM

DNA probe signals were captured by one-step system detection of biotin- labelled probe with streptavidin-CAGE590 (Abberior), and one-step system detection of digoxigenin- labelled probe with anti-digoxigenin-Alexa Fluor 647 (Jackson ImmunoResearch).

iPALM imaging and post-processing

The samples for iPALM were imaged in STORM buffer[28], using coverslips with fiducial markers, prepared according to Shtengel et al.[25]. 3D-FISH samples were imaged using non-commercial iPALM system[24] available at Advanced Imaging Center– HHMI's Janelia Research Campus, with excitation: 647nm laser (5.5 kW/cm^2) and 561nm laser (4.5 kW/cm^2) and activation: 405nm laser (100W/cm^2). The number of frames is 25000, and the exposure time is about 50ms. iPALM data was processed to extract single molecule 3D coordinates and localization precisions, and subsequently visualized using the PeakSelector software (Janelia Research Campus)[25]. FISH signals acquired by iPALM were segmented based on the threshold with custom-made software PartSeg (https://4dnucleome.cent.uw.edu.pl/PartSeg/). Then, 3D reconstructions were obtained using Imaris (Bitplane).

Cell preparation for 3D-EMISH

The experiments were performed on cultured GM12878 cells. After centrifugation, fixation of the cell pellet (~7x10^7 cells) with 4% paraformaldehyde in PBS overnight at 4□C and washing with PBS, the artificial tissue with embedded cells was formed. To the fixed and washed pellet, 0.2 ml the fibrinogen solution (100 mg fibrinogen (Sigma; F3879), 53.33 mg sodium citrate, 283.33 mg sodium chloride, 33.33 ml H_20) was added and stirred. After

centrifugation, 0.2 ml the thrombin solution (Sigma; T7009-100UN + 1ml H_20) was added[29]. The clot was postfixed with 4% paraformaldehyde in PBS (10 min; RT) and washed with PBS. Then, the formulated artificial tissue was soaked with 30% sacharose in PBS overnight at 4□C and frozen in Tissue Freezing Medium (Leica). After overnight storage at -80□C, the clot was cut into 40 µm slices using cryostat (Leica).

In situ hybridization for 3D-EMISH

In situ hybridization was performed on the free floating sections of the clot according to Cremer et al.[27], with modifications. The sections were washed with PBS (3 x 5 min; RT), 0.5% Triton X-100 (Sigma) in PBS (1 x 20 min; RT), 2xSSC (2 x 2 min; 37□C), incubated with 0.1 mg/ml RNase A in 2xSSC (Sigma; R6513) (10 min; 37□C), washed with 2xSSC (2 x 2 min; 37□C), incubated with citrate buffer pH 6 (30 min, 80□C), cooled down to room temperature and washed with 2xSSC (2 x 5 min; RT). After that, blocking of endogenous biotin was performed using the Avidin/Biotin Blocking Kit (Vector Laboratories; SP-2001), by incubation with Avidin D (four drops of the Avidin D solution to 1 ml 2xSSC) (15 min; RT), briefly washing with 2xSSC and incubation with the biotin solution (four drops of the biotin solution to 1 ml 2xSSC) (15 min; RT), followed by washing with 2xSSC (2 x 5 min; RT) and incubated with 50% formamide in 2xSSC overnight at 4□C. After this step, the sections and biotin-labelled DNA probes were overlaid with a glass chamber, sealed with rubber cement, prehybridized (4h, 45□C), denatured (5 min, 80□C) and hybridized (48h, 37□C). After two-days hybridization, sections were washed with 2xSSC (2 x 10 min; 37□C; with shaking), 0.1xSSC (2 x 10 min; 60□C; with shaking), incubated with blocking solution- 4% BSA (Sigma), 0.2% Tween (Sigma), 4x SSC (1h, 37□C) following incubation with Alexa Fluor™ 488 FluoroNanogold™-Streptavidin (Nanoprobes; 7216) in 2% BSA (Sigma), 0.2% Tween (Sigma), 4x SSC (overnight; 4°C; with shaking - concentration 0.8 µg/ml) and washed

with 0.2% Tween (Sigma) in 4xSSC (3 x 10 min, RT; with shaking). After hybridization and washing, sections were mounted in 2xSSC buffer and imaged with the Zeiss LSM 780 confocal microscope using the 488 nm argon laser and the water objective (C-Apochromat 40x/1.2 W Corr FCS). Only sections containing nuclei with well visible FISH signals were processed to 3D-EMISH.

3D-EMISH staining

Sections after passing the quality control using confocal microscopy were washed with ddH_20 (5 x 3 min; RT) and incubate with silver enhancement kit to increase size of 1.4 nm nanogold particles (4 x 10 min; RT; LI Silver Enhancement Kit (Molecular Probes; L-24919)) and washed tightly with ddH_20. After silver enhancement, sections were postfixed with 2.5% glutaraldehyde in 0.1M cacodylate buffer (Sigma) (2 h; RT), washed with 0.1M cacodylate buffer (Sigma) (3 x 10 min; RT), incubated with 1% tannic acid in 0.1M cacodylate buffer (Sigma) (2 x 2h; 4°C), washed with water (5 x 3 min; RT) and incubated with 4% uranyl acetate in 50% ethanol (overnight; RT). Then the dehydration was performed using increasing concentration of ethanol: 50%, 60%, 70%, 80% and 95% (1 x 15 min each; RT), absolute ethanol (2 x 20 min; RT). After dehydration, sections were prepared to embedding by incubation with acetone (2 x 10 min; RT), increasing the ratio of Epon (Sigma)/acetone mix: 1:3, 1:1, 3:1 (1h each; RT), and Epon (1 h; RT and then overnight; RT). The next day, Epon was replaced with fresh one and specimens were embedded between two sheets of ACLAR® Film and placed into 60□C oven (24-48 h). After polymerization of the resin, the sample was cut with razor blade and scalpel, glued on pin (metal rivet; Oxford Instruments) with silver conductive resin (CircuitWorks), and incubated 2 hours at 65□C. Using ultramicrotome (Leica) and diamond knife (DiATOME) smooth surface of sample to SBF-SEM was obtained. Then, to enhance conductivity, sides of the sample were painted with silver paint (Ted Pella).

EM imaging

To image 3D-EMISH samples, Zeiss Sigma electron microscope with backscatter electron detector and ultamicrotome with diamond knife inside the chamber was used (3View2 from Gatan). All images were collected using variable pressure mode with EHT 4-6kV, aperture 30 µm and resolution 8192x8192 pixels. Replicate 1 was collected with pixel size 7 nm, sliced each 50 nm, 300 times (voxel size: 7x7x50 nm). Replicate 2 was collected with pixel size 5 nm, sliced each 30 nm, 600 times (voxel size: 5x5x30 nm). To examine potential harmful effect of reagents on nuclear ultrastructure, transmission electron microscope JEM 1400 (JEOL) was used.

3D reconstructions of 3D-EMISH images

First, nuclei were segmented manually and 3D-reconstructed using Amira (FEI). Second, 3D-EMISH target chromatin structures in a nucleus were segmented and reconstructed in 3D objects using Amira (FEI) or segmented using PartSeg (https://4dnucleome.cent.uw.edu.pl/PartSeg/) and 3D-reconstructed using UCSF Chimera software[30].

Image processing and quantitative analysis

All 3D electron microscopy stacks were preprocessed with ImageJ plugin – Linear Stack Alignment with SIFT[31]. The images were manually inspected, and then a cuboid containing the region of interest (ROI) was cut. The mask defining the ROI was determined by connecting component analysis of objects inside the cuboid. We took the largest connected component using custom made software, where we used Maximum Entropy algorithm (ImageJ plugin) to optimize the threshold value to segment the structure. The resulting mask

was overlaid on the image to segment the structure. Subsequently, 3D images were resampled in order to obtain the same voxel size (5 nm) in x, y, and z. The reslicing was performed by upsampling with linear interpolation between adjacent planes. We also applied a gaussian filter of size 1 pixel (i.e. 5 nm) in the x-y planes in order to remove possible pixel noise. The isotropic scale was required by the plugin used to produce the movies (with unequal scales the structures appear in the movies unnaturally flattened), and also it was needed by the algorithm for morphological domains separation, which operates on a cubical grid. The upsampling is not obviously visible unless we rotate the structure through an angle perpendicular to the axial direction, in the supplementary movies the structures were rotated through an axis perpendicular to its longest (principle) axis, which in general is randomly oriented with respect to the slicing direction Then, Gaussian fliter (5 nm cut-off size) was applied to each z-section to remove the detector noise. The volume (V) and surface (S) of the segmented structure were calculated by 3D Object Counter plugin (ImageJ). The form factor (ff) was defined as

$$\mathrm{ff} = (36\,\pi)^{-\frac{1}{3}}\,\mathrm{S}\,\mathrm{V}^{-\frac{2}{3}},$$

where the value is 1 for a spherical object and increase as the structure is less compact than a sphere. For illustrative purpose, the segmented structures were aligned accordingly to their principal axis[32]. The structures were classified into 5 different morphological groups: 1 compact sub-domain group (one spherical ball shape), 2 distinctive sub-domain group (dumbbell shape), and 3 - 5 distinctive sub-domain groups by applying the following sub-domain identification algorithm.

First, the structure was smoothed out by applying the “maximum filter” with 135 nm cut-off size. This parameter was experimentally tested and determined to prevent from over-segmenting sub-domains of a structure , yet preserving the overall morphological feature. Second, the local maximal density centers were calculated per each identified distinctive

group. Third, these local maxima were subsequently used as seed points in computing of the diffusion process, where the image density was used as a local diffusion coefficient. The diffusion process was simulated by solving numerically an uncoupled set of diffusion equations,

$$\partial u_i(\vec{r},t)\ \partial t\ =\ \nabla\cdot\ D(u_i(\vec{r},t),r)\nabla u_i(\vec{r},t).$$

where u_i denotes the density of the diffusing material, and D denotes the EMISH signal density, i=1...N (the number of seed points) , $\vec{r}$ are the pixel coordinates in 3D space.

Initially, we assume that all EMISH signals of each sub-domain was concentrated in each seed point. We represented it as normalized gaussian functions centered at the seed points. Image voxels, diffused from the same seed point, belong to the same sub-domain group. The 3D image region of low EMISH signal density will diffuse slower than that of high EMISH signal density. The boundary voxels had diffused signals from two or more different seed points, and these boundary voxels belong to the sub-domain group which is the highest diffused signal. The diffusion process was completed when all voxels were filled by a non-zero density and the structure was divided into separate sub-domains.

Statistical analysis

Statistical analysis was performed using IBM SPSS Statistics software. In all cases, error bars indicate SEM. The morphological feature statistics of 3D-EMISH structures for different sub-domain groups was performed using Kruskal-Wallis test with Bonferroni post-hoc test. Statistically insignificant comparison was marked as ns, and statistically significant differences were marked with asterisks: * $p \leq 0.05$; ** $p \leq 0.01$; *** $p \leq 0.001$.

For the three-dimensional ROI, we created the following binary masks: specific signal mask (SP), non-specific background signal mask (NS) and no-signal background mask (BN). The

specific and non-specific signal volume, was obtained by summing all mask elements for SP and NS masks respectively, and multiplying it by the voxel volume. The content of the unspecific signal in the background volume was obtained as a ratio of NS mask volume, and the total background volume (sum of NS and BN mask volumes).

Code and Data availability

3D-EMISH image processing code and data files are available at the following public repository server: https://github.com/3DEMISH/3D-EMISH

Acknowledgments

This work was primarily supported by the Human Frontier Science Program, grant no. RGP0039/2017 (to YR and GMW). GMW is also supported by the grants from Polish National Science Center no. UMO-2013/08/M/NZ3/00655. PT is also supported by a Polish National Science Centre Grants 2014/15/N/NZ2/00379 and 2017/24/T/NZ2/00307. YR and BL are also supported by 4DN (U54 DK107967) and ENCODE (UM1 HG009409) consortia. DP, GB, MK, ZP are supported by Polish National Science Centre (2014/15/B/ST6/05082), Foundation for Polish Science co-financed by the European Union under the European Regional Development Fund (TEAM to DP), and by 4DN (U54 DK107967). KKP is partially supported by ETIUDA grant from Polish National Science Centre no. UMO-2019/32/T/NZ4/00502. AM is partially supported by Sonata bis grant from Polish National Science Centre UMO-2015/18/E/NZ3/00730 . iPALM imaging was conducted in collaboration with the Advanced Imaging Center at Janelia Research Campus of Howard Hughes Medical

Institute. This work has been also supported by Polish National Science Centre (2014/15/B/ST6/05082), Foundation for Polish Science co-financed by the European Union under the European Regional Development Fund (TEAM to DP).

Author contributions

GMW and YR conceived and supervised the project. PT and BL designed the experiments. PT performed the 3D EMISH experiments under GMW's supervision, and generated the raw imaging data with KK's assistance. BR developed the sub-domain identification algorithm and processed them. PT, BR, KKP, GB, KK, interpreted and processed the raw data. BR, KKP, GB, MK performed post-processing of EMISH images, and/or statistical analysis. BR and KKP designed and performed the detection of morphological domains in the EMISH-detected structures. JA executed iPALM imaging, together with PT and GMW. MS and AAS participated in EMISH imaging. Artur Wolny contributed to the manuscript figures. Agnieszka Walczak participated in the initial design of EMISH hybridization. AM, ZP, and DP provided remarks to the discussion on experimental strategy. PT wrote the first draft of the manuscript. YR, BL, GMW, BR, PT and KKP extensively edited the manuscript. MKA and SA acquired, reconstructed, segmented, visualized electron tomography data and accordingly added it to the manuscript. All authors revised the final manuscript.

Competing Financial Interests

There is no competing financial interest

The authors declare no competing interests.

References

1. Li, G. *et al.* Extensive Promoter-Centered Chromatin Interactions Provide a Topological Basis for Transcription Regulation. *Cell* **148**, 84–98 (2012).
2. Pope, B. D. *et al.* Topologically associating domains are stable units of replication-timing regulation. *Nature* **515**, 402–405 (2014).
3. Lieberman-Aiden, E. *et al.* Comprehensive Mapping of Long-Range Interactions Reveals Folding Principles of the Human Genome. *Science* **326**, 289–293 (2009).
4. Dekker, J., Marti-Renom, M. A. & Mirny, L. A. Exploring the three-dimensional organization of genomes: interpreting chromatin interaction data. *Nat. Rev. Genet.* **14**, 390–403 (2013).
5. Fullwood, M. J. *et al.* An oestrogen-receptor-α-bound human chromatin interactome. *Nature* **462**, 58–64 (2009).
6. Giorgetti, L. & Heard, E. Closing the loop: 3C versus DNA FISH. *Genome Biol.* **17**, (2016).
7. Rao, S. S. P. *et al.* A 3D Map of the Human Genome at Kilobase Resolution Reveals Principles of Chromatin Looping. *Cell* **159**, 1665–1680 (2014).
8. Dixon, J. R. *et al.* Topological domains in mammalian genomes identified by analysis of chromatin interactions. *Nature* **485**, 376–380 (2012).
9. Sexton, T. & Cavalli, G. The Role of Chromosome Domains in Shaping the Functional Genome. *Cell* **160**, 1049–1059 (2015).
10. Tang, Z. *et al.* CTCF-Mediated Human 3D Genome Architecture Reveals Chromatin Topology for Transcription. *Cell* **163**, 1611–1627 (2015).
11. Phillips, J. E. & Corces, V. G. CTCF: Master Weaver of the Genome. *Cell* **137**, 1194–1211 (2009).
12. Combs, C. A. Fluorescence Microscopy: A Concise Guide to Current Imaging Methods. in *Current Protocols in Neuroscience* (eds. Crawley, J. N. et al.) (John Wiley & Sons, Inc., 2010). doi:10.1002/0471142301.ns0201s50.

13. Cremer, T. & Cremer, M. Chromosome Territories. *Cold Spring Harb. Perspect. Biol.* **2**, a003889–a003889 (2010).
14. Trask, B. J. Human cytogenetics: 46 chromosomes, 46 years and counting. *Nat. Rev. Genet.* **3**, 769–778 (2002).
15. Boettiger, A. N. *et al.* Super-resolution imaging reveals distinct chromatin folding for different epigenetic states. *Nature* **529**, 418–422 (2016).
16. Szabo, Q. *et al.* TADs are 3D structural units of higher-order chromosome organization in *Drosophila*. *Sci. Adv.* **4**, eaar8082 (2018).
17. Bintu, B. *et al.* Super-resolution chromatin tracing reveals domains and cooperative interactions in single cells. *Science* **362**, eaau1783 (2018).
18. Manuelidis, L. Different central nervous system cell types display distinct and nonrandom arrangements of satellite DNA sequences. *Proc. Natl. Acad. Sci.* **81**, 3123–3127 (1984).
19. Solovei, I. *et al.* Spatial Preservation of Nuclear Chromatin Architecture during Three-Dimensional Fluorescence in Situ Hybridization (3D-FISH). *Exp. Cell Res.* **276**, 10–23 (2002).
20. Ou, H. D. *et al.* ChromEMT: Visualizing 3D chromatin structure and compaction in interphase and mitotic cells. *Science* **357**, eaag0025 (2017).
21. Cremer, M. *et al.* Multicolor 3D Fluorescence In Situ Hybridization for Imaging Interphase Chromosomes. in *The Nucleus* (ed. Hancock, R.) vol. 463 205–239 (Humana Press, 2012).
22. Rouquette, J. *et al.* Revealing the high-resolution three-dimensional network of chromatin and interchromatin space: A novel electron-microscopic approach to reconstructing nuclear architecture. *Chromosome Res.* **17**, 801–810 (2009).
23. Denk, W. & Horstmann, H. Serial Block-Face Scanning Electron Microscopy to Reconstruct Three-Dimensional Tissue Nanostructure. *PLoS Biol.* **2**, e329 (2004).
24. Shtengel, G. *et al.* Interferometric fluorescent super-resolution microscopy resolves 3D cellular ultrastructure. *Proc. Natl. Acad. Sci.* **106**, 3125–3130 (2009).

25. Shtengel, G. *et al.* Imaging cellular ultrastructure by PALM, iPALM, and correlative iPALM-EM. in *Methods in Cell Biology* vol. 123 273–294 (Elsevier, 2014).
26. Gibcus, J. H. *et al.* A pathway for mitotic chromosome formation. *Science* **359**, eaao6135 (2018).
27. Cremer, M. *et al.* Multicolor 3D Fluorescence In Situ Hybridization for Imaging Interphase Chromosomes. in *The Nucleus* (ed. Hancock, R.) vol. 463 205–239 (Humana Press, 2012).
28. Dempsey, G. T., Vaughan, J. C., Chen, K. H., Bates, M. & Zhuang, X. Evaluation of fluorophores for optimal performance in localization-based super-resolution imaging. *Nat. Methods* **8**, 1027–1036 (2011).
29. Glauert, A. *Practical methods in electron microscopy*. (North Holland Publishing Company, 1972).
30. Pettersen, E. F. *et al.* UCSF Chimera?A visualization system for exploratory research and analysis. *J. Comput. Chem.* **25**, 1605–1612 (2004).
31. Lowe, D. G. Distinctive Image Features from Scale-Invariant Keypoints. *Int. J. Comput. Vis.* **60**, 91–110 (2004).
32. Abdi, H. & Williams, L. J. Principal component analysis: Principal component analysis. *Wiley Interdiscip. Rev. Comput. Stat.* **2**, 433–459 (2010).

Figure legends

Fig. 1| 3D-EMISH method to visualize ultra-resolution 3D chromatin folding

a, 3D-EMISH schematic. Cells are grown in suspension. After fixation with 4% PFA, thrombin-fibrinogen clot is formed. The clot is post-fixed, soaked with cryoprotectant, frozen and cut in 40 µm sections. Free-floating sections are subjected to in situ hybridization with biotinylated DNA probe and processed to SBF-SEM. Then, multiple rounds of ultra-thin slicing and imaging are performed. Each cubical sample volume contains dozens of cells. Cell nucleus is segmented, containing two separated target chromatins, as an example in 3D-EMISH. **b**, Image processing for 3D-EMISH. First, we searched the connected components through z-stack images per each identified nucleus (blue dotted circle). Second, the chromatin target structures were identified by removing unspecific background EM signals. EM signals, connected in multiple consecutive layers were considered as actual target chromatin bound signals, otherwise regarded as chromatin unbound signals, or unspecific signals. Two scale bars are 1 µm. **c**, 3D-EMISH image example of one slice and all z stack projected image after filtering out background EM signals. Two scale bars are 200 nm. **d**, 3D reconstructed chromatin folding structure examples. We assigned unique structure index number (sID) for each structure; scale bar, 500 nm.

Fig. 2| 3D-EMISH chromatin image collection for 1.7Mb target genomic region

a, Genome browser view of the target region in hg38, Chr7:141,547,153-143,237,066, in GM12878 cells. From top to bottom, 2D contact map (CTCF ChIA-PET, 5Kb resolution), three distinctive loop domains (141,547,153 – 141,786,415; 141,975,791 – 142,304,141; 142,463,980 – 143,237,066), loop and peak for CTCF ChIA-PET, loop and peak for RNAPII ChIA-PET, RNA-seq, and DNA probes using BAC clone for 3D-EMISH and two color FISH. **b**, Confocal microscopy image of the target genomic region using two color DNA-FISH (left) and

3D reconstructed FISH signals (right). **c**, Cross-section illustration of 3D-EMISH cubical samples, where the dotted black square represents the sample boundary. Cells contain either two target chromatins in a nucleus (G1 phase) or four target chromatins in a nucleus (S-M phase). 3D-EMISH collected whole cell nuclei (W, orange), located at the inner cubic sample, and truncated nuclei (T, blue), located at the outer cubic sample. Intact target chromatin folding structures (green dots) were collected. Truncated partial structures and structures beyond the cubical sample were not collected, represented as red dots. Total 229 target chromatin folding structures were collected from two replicates, containing 26 whole nuclei and 140 truncated nuclei. **d**, Examples of collected target chromatin folding structures with their nuclei are presented. From top to bottom, 1(T), 2(T), 2(W), 3(T), and 4(W) structures per a nucleus are shown with structure index numbers (sID, details in supplementary table and supplementary figure 3). **e**, Nucleus count for 1, 2, 3, and 4 structures per a nucleus.

Fig. 3| 3D-EMISH distinctive chromatin folding domain identification

a, 3D-EMISH image processing steps to identify distinctive chromatin folding domain. We smooth out 3D-EMISH image to remove fine-grain feature, search distinctive folded sub-domains, and calculate the center point of each domain, represented as red dots. Applying diffusion process, starting from each center point to cover all voxels in 3D image, we identified each chromatin folding domain in the 3D-EMISH chromatin image. For the example chromatin structure (sID 172), three local density centers were identified, and then three distinctive chromatin folding domains were identified, presented in three different colors (magenta, green, and cyan); scale bar, 500 nm. **b**, Three typical examples of 3D-EMISH chromatin image are shown, single condensed chromatin folding domain (sID 50, supplementary movie 1), two distinctive chromatin folding domains (sID 12, supplementary

movie 2), and three distinctive chromatin folding domains (sID 42, supplementary movie 3) for three different view angles (xy, xz, and zy from left to right) with identified local density centers (red dots) with projected density signal curves on each axis. **c**, Identified individual chromatin folding domains are distinguished by different colors (magenta for the first domain, green for the second domain, and cyan for the third domain); scale bar, 500 nm.

Fig. 4| 3D-EMISH statistical analysis of chromatin folding domains.

a, Classified 1, 2, 3, 4 distinctive chromatin folding domains examples. Identified chromatin folding domains in each 3D image were presented by different colors (magenta, green, cyan, and yellow for first, second, third, and fourth domain group, respectively); scale bar, 500 nm. **b,** 3D-EMISH chromatin folding domain histogram of 229 structures: 1 domain (58/229, 25%), 2 domains (90/229, 39%), 3 domains (70/229, 31%), 4 domains (11/229, 5%). Volume (**c**), surface area (**d**), and form factor (**e**) statistics for all 229 images for four distinctive classified chromatin folding domains. Error bar indicates SEM. Kruskal-Wallis test, and Bonferroni post-hoc test; ns (statistically insignificant); statistically significant differences: * $p \leq 0.05$; ** $p \leq 0.01$; *** $p \leq 0.001$.

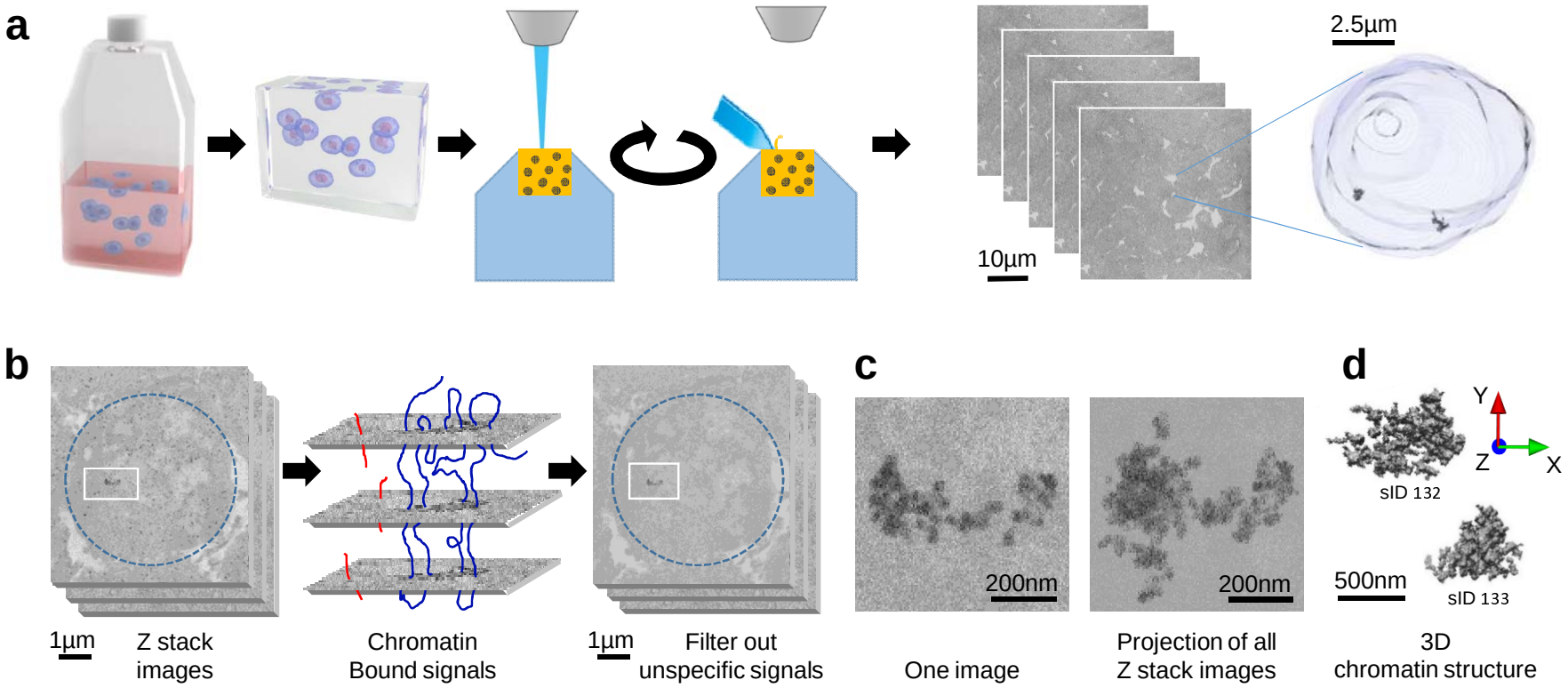

g. 1

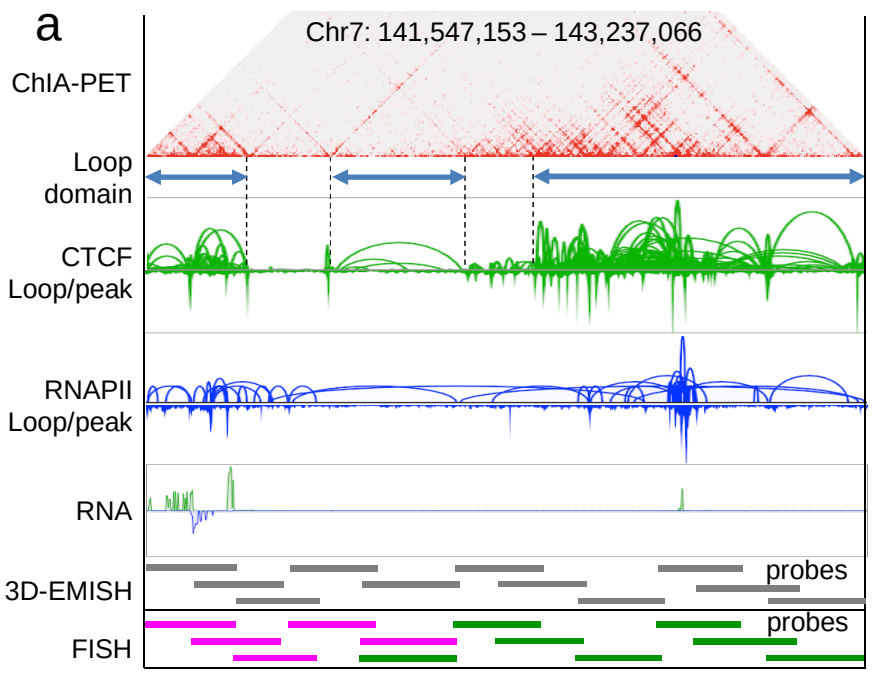

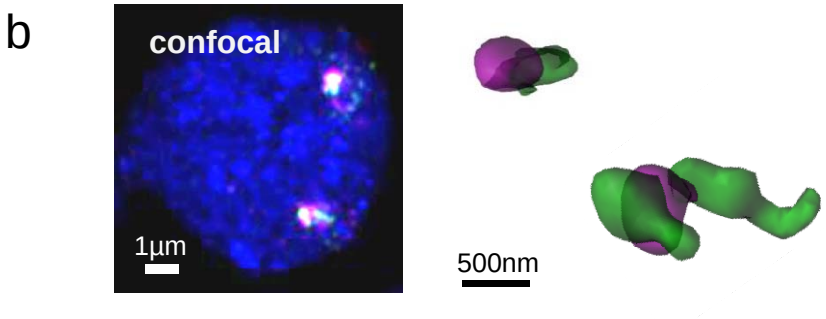

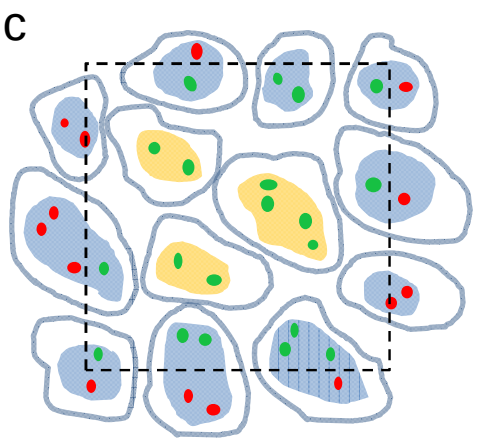

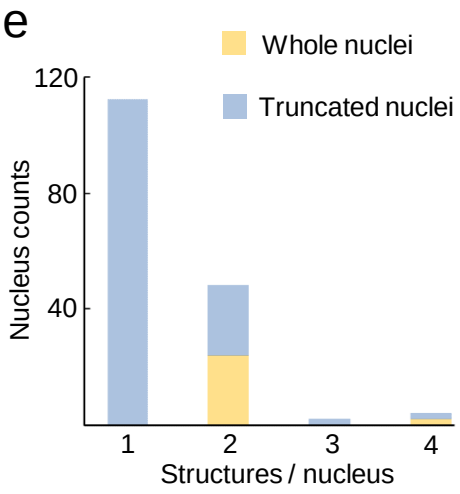

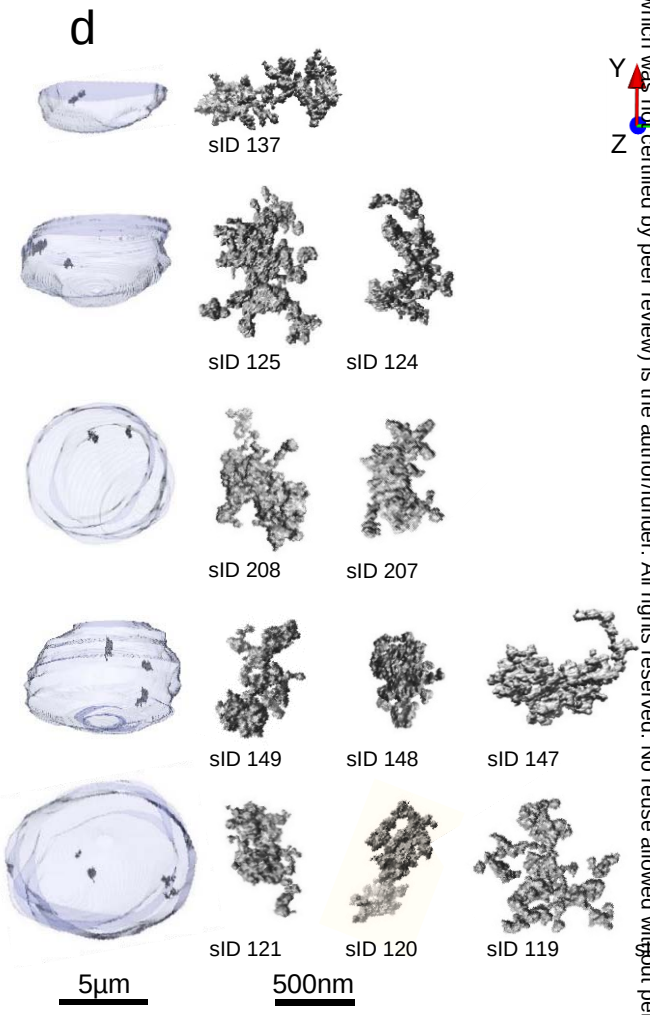

g. 2

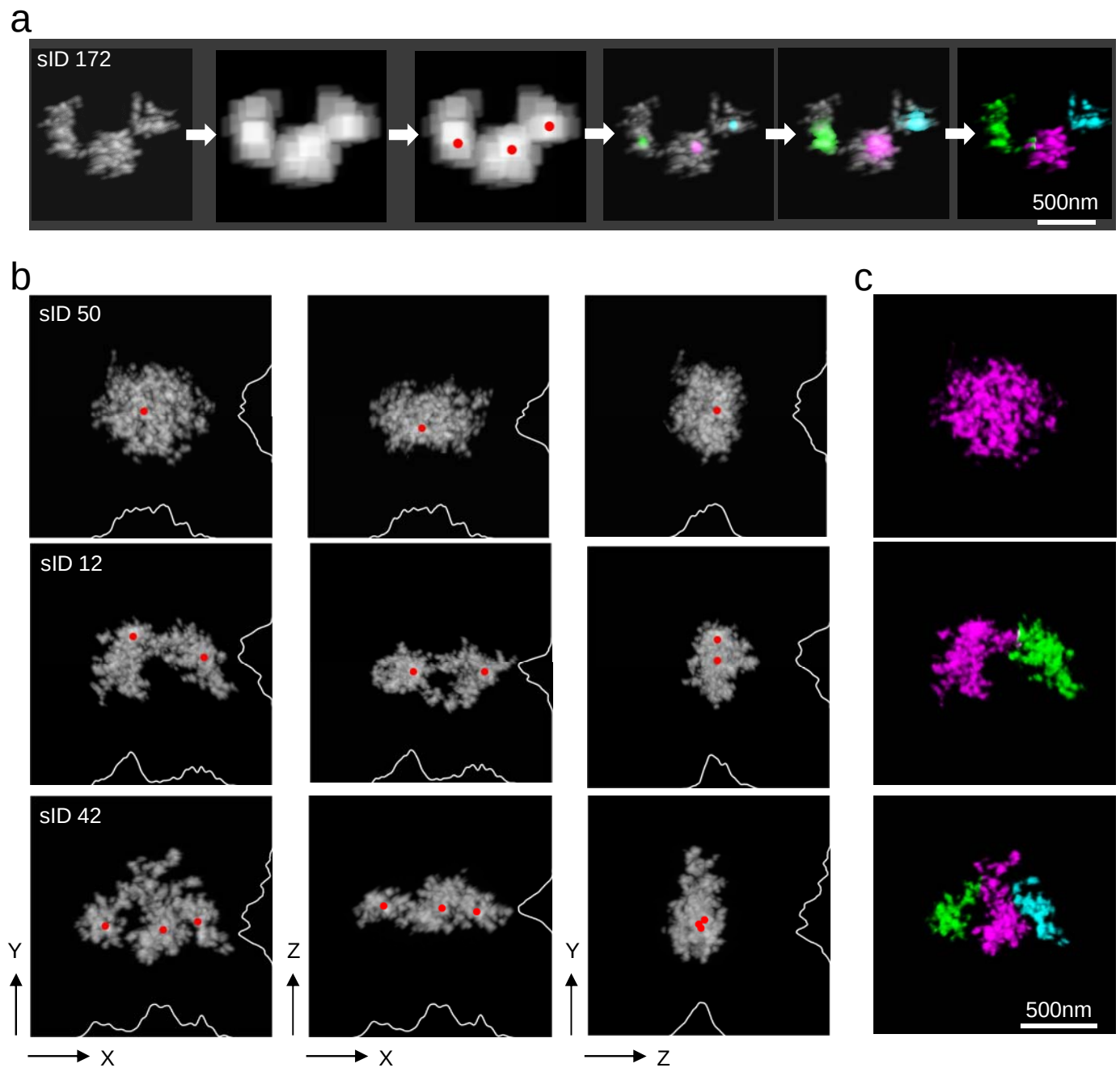

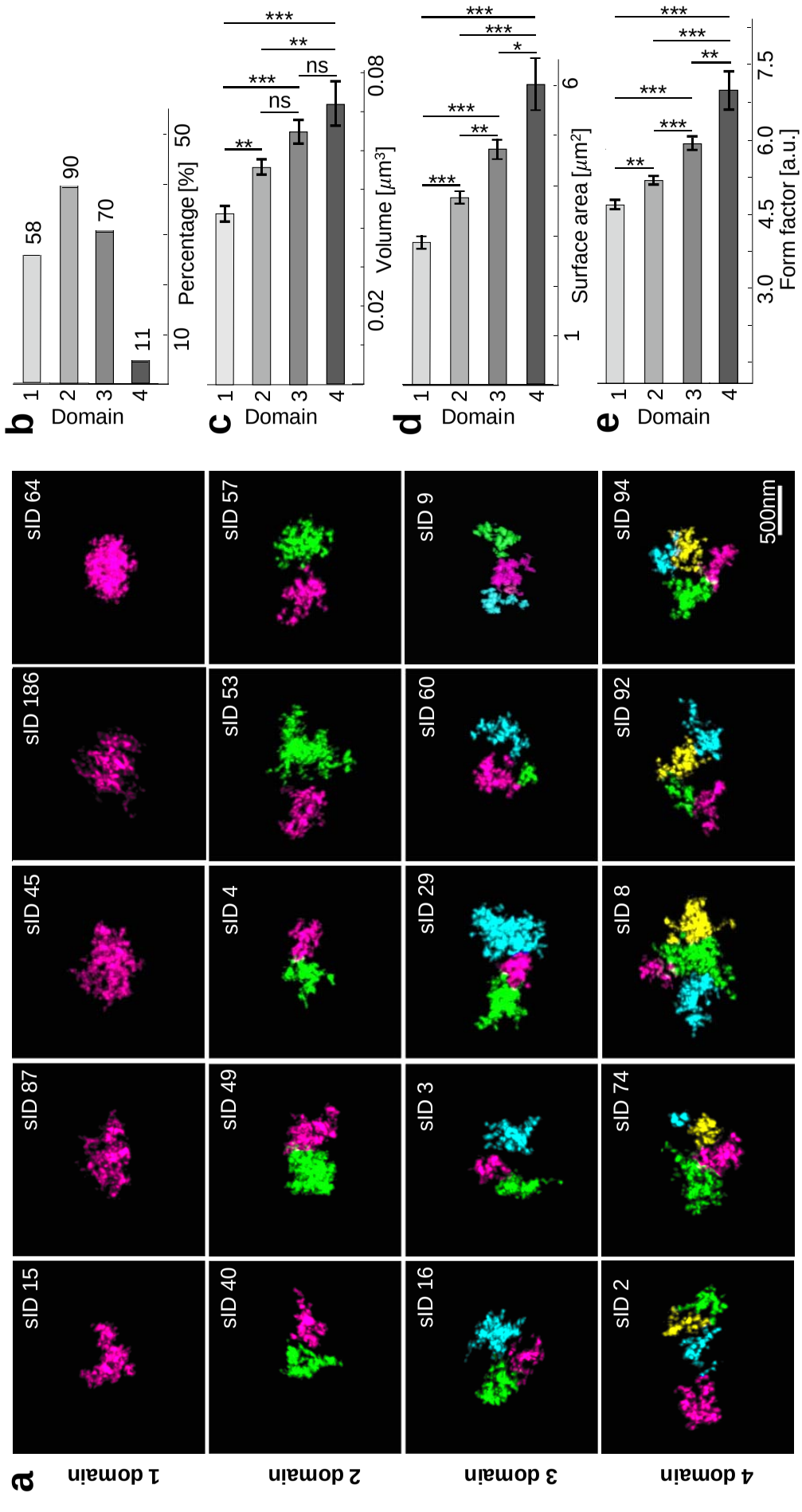

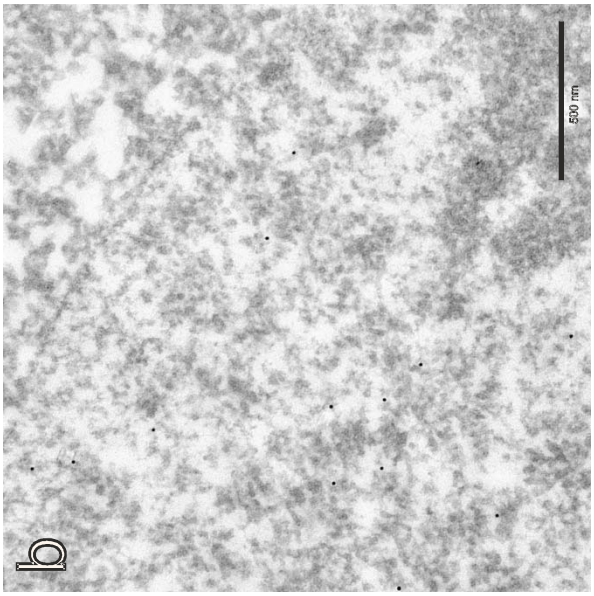

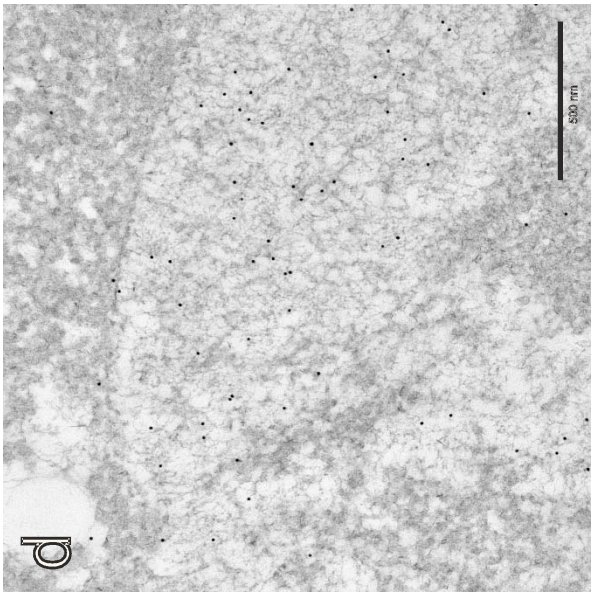

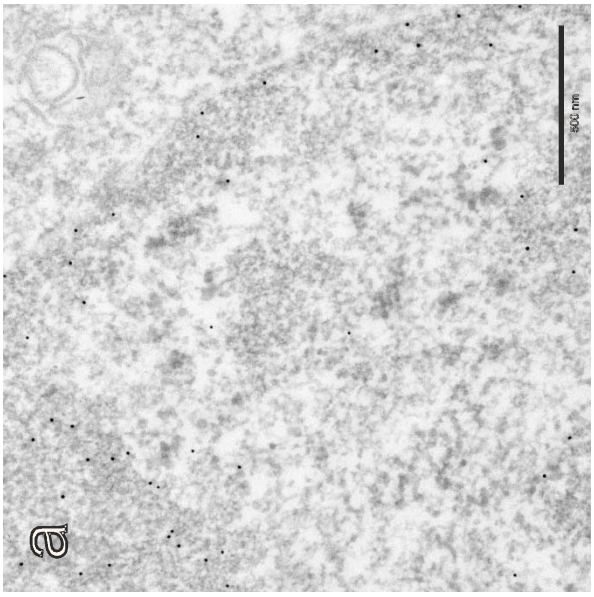

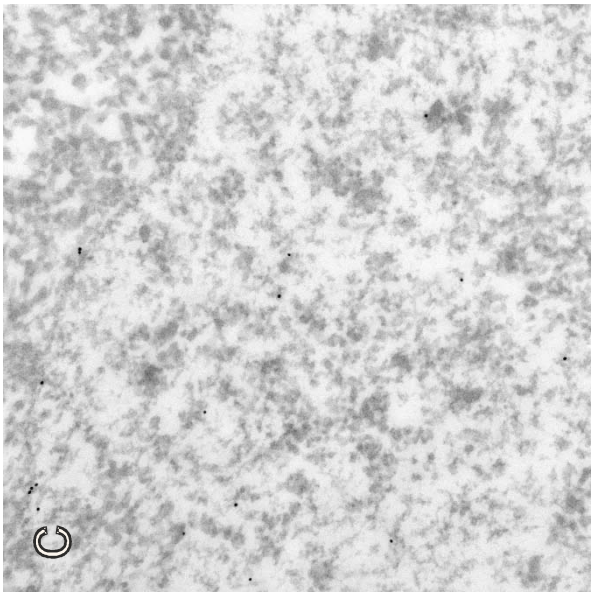

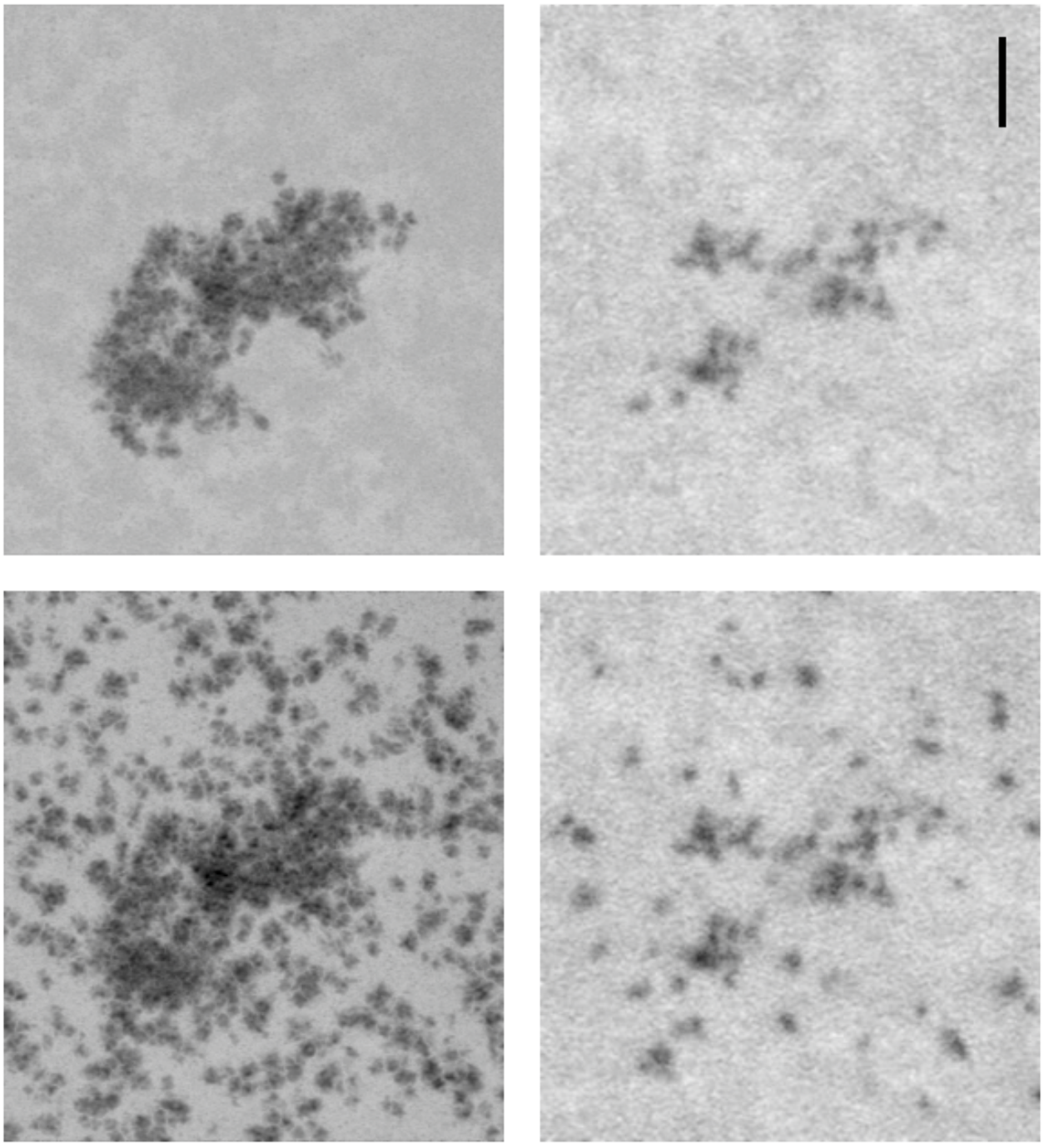

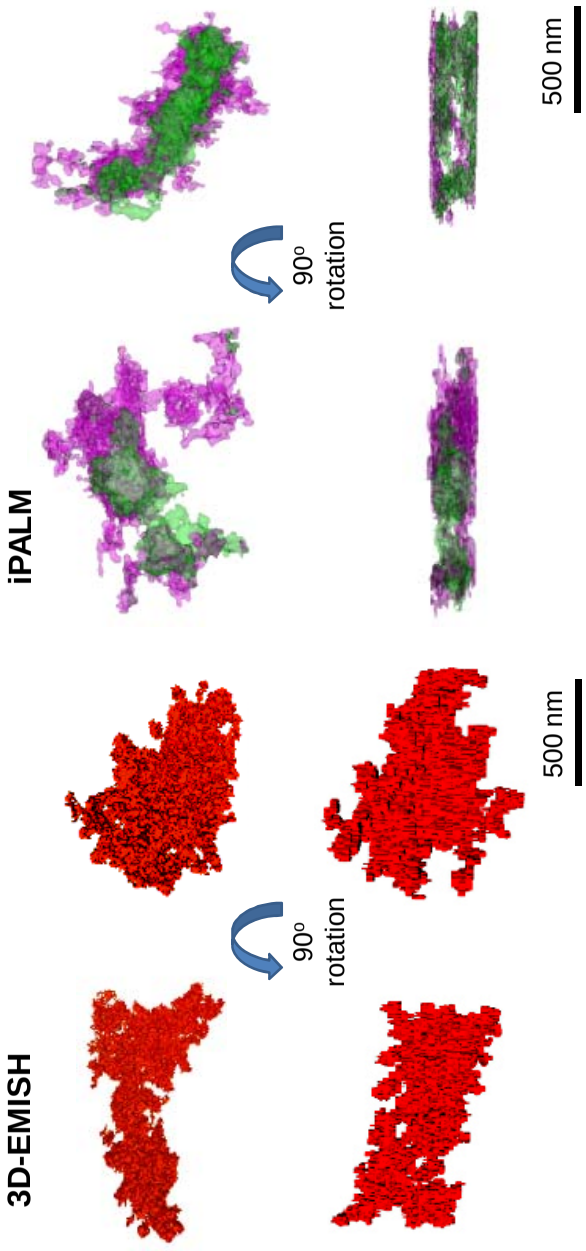

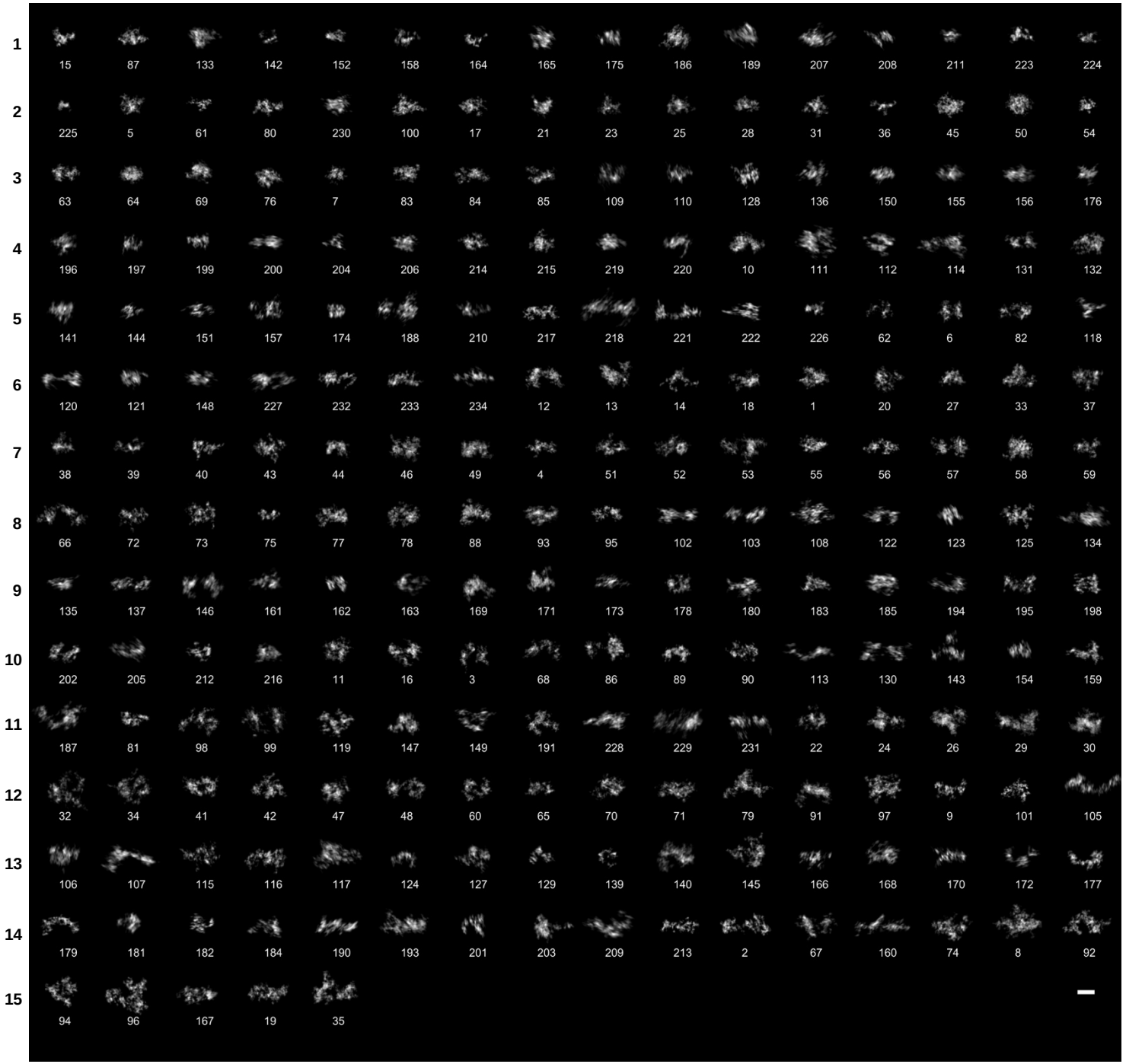

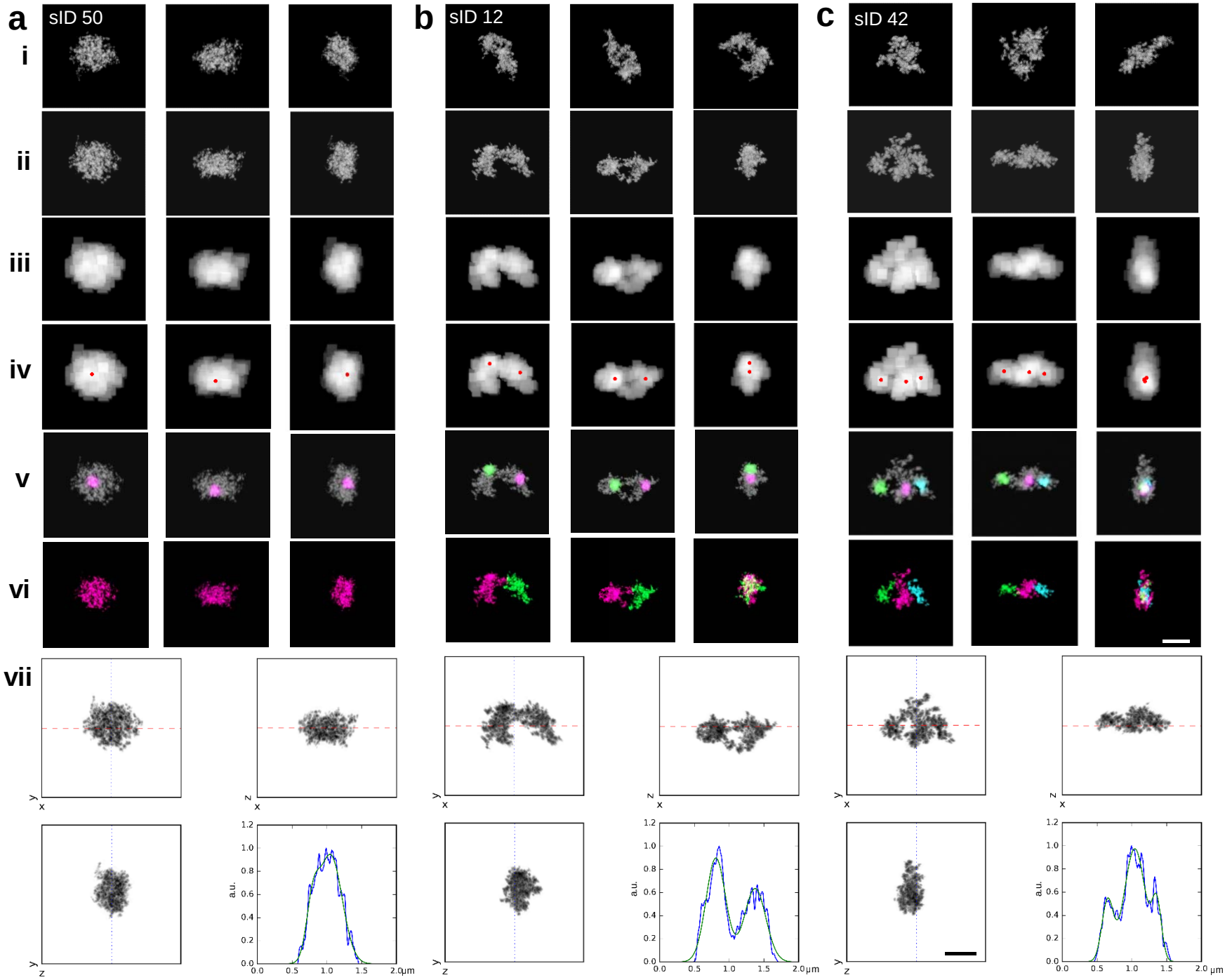

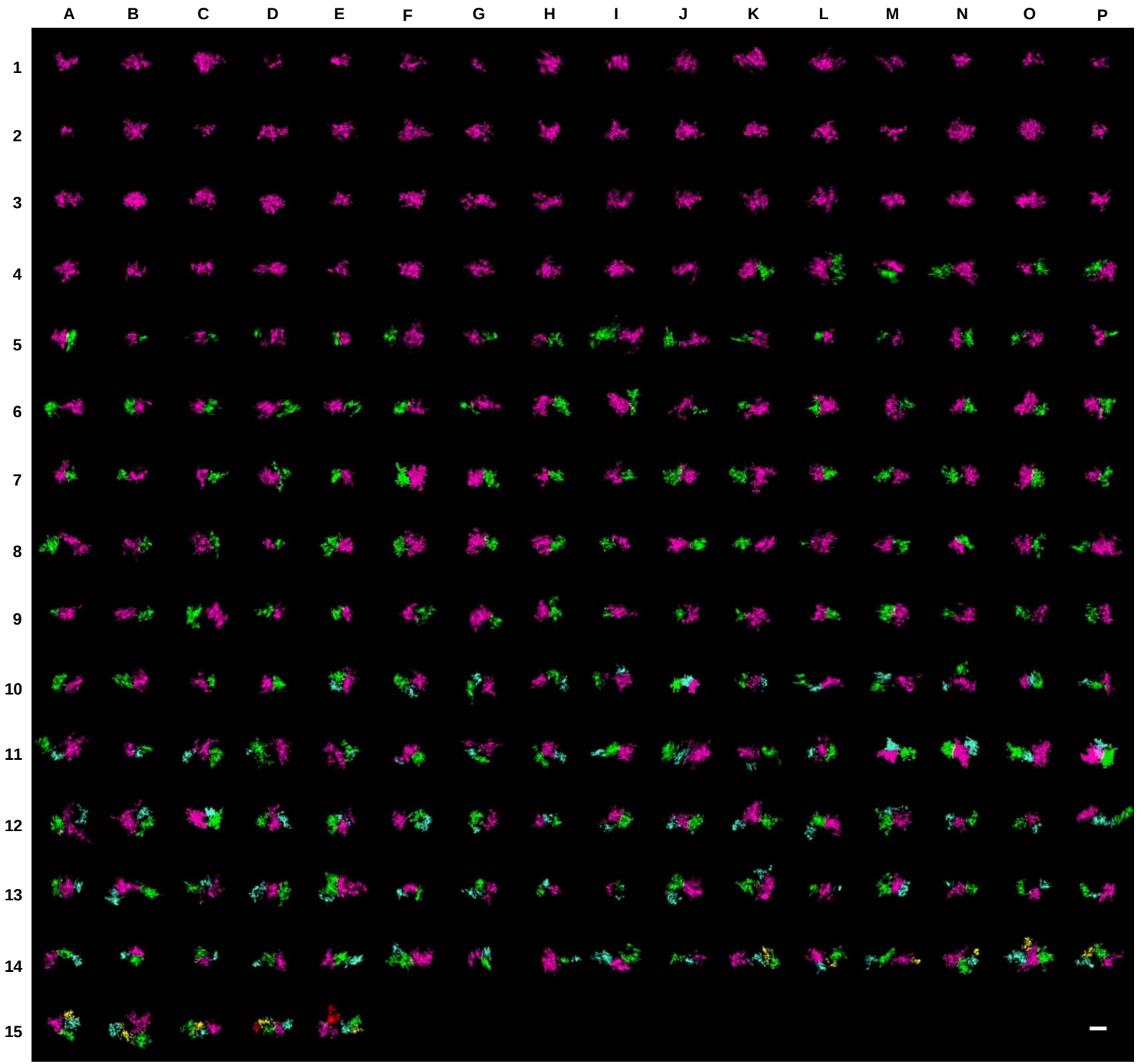

Fig. S8